

Article

Influence of Fatty Acid Alkyl Chain Length on Anisotropy of Copper Nitride Nano-Crystallites

Takashi Nakamura

Research Institute for Chemical Process Technology, National Institute of Advanced Industrial Science and Technology (AIST), Nigatake 4-2-1, Miyagino-ku, Sendai 983-8551, Japan; nakamura-mw@aist.go.jp; Tel.: +81-29-861-2272

Academic Editor: Rainer Niewa

Received: 30 September 2016; Accepted: 11 January 2017; Published: 16 January 2017

Abstract: My group developed a simple method to prepare copper nitride fine particles from copper carboxylate in a solvent of long-chain alcohols without the use of high temperatures or high pressures. By selecting copper acetate or copper decanoate as the copper source, my group demonstrated that the morphology of the copper nitride fine particles varied between cubic and plate-like, respectively. Although a hypothesis was proposed to explain the influence of the length of the alkyl chain on the copper decanoate, it is uncertain how much the chain length influences the shape of the fine particles. In this work, I demonstrated the effect of the length of the alkyl chain on particle shape by preparing fine particles from a series of copper sources with different alkyl chain lengths and characterizing the particles with x-ray diffractometry (XRD), scanning electron microscopy (SEM), and transmission electron microscopy (TEM). The main findings were as follows: (1) the fine particles were plate-like when the alkyl chain length exceeded 5; (2) the aspect ratio of the plate-like particles increased as the alkyl chain length increased; and (3) growth of the (110) and (111) planes of the copper nitride crystal were selectively inhibited.

Keywords: copper; nitride; anisotropy; morphology control; nanoparticle; crystal plane

1. Introduction

To elicit high performance from inorganic crystals with respect to their catalytic [1–3] and photonic properties [4–6], it is important to understand the chemical conditions on the crystal surface and to control the crystal planes. Investigating the relationship between the crystal surface and crystal functionality is facilitated with the use of fine particles. One goal of catalyst research is to increase the proportion of chemically active atoms on the catalyst surface. Differences in catalytic efficiency due to variations of the crystal planes are therefore very important. In studies of the optical properties of inorganic crystals, quantum size effects are important when fine particles, especially nanoparticles, are being used. The relationship between crystal shape and light (electromagnetic waves) can be evaluated with knowledge of quantum chemistry.

In studies of the use of colloids and fine particles for inorganic crystals, the morphologies of crystallites and particles have often been controlled by using surface modifiers [7,8]. In such cases, the phenomenon of selective adsorption of the surface modifier to a specific crystal face is utilized. The reaction temperature used to prepare the particles is also an important regulator of particle size when modifiers are used. Changes in crystal shape arise from the balance between the thermodynamic stability of the crystal at a given temperature and the suppression of growth of the specific crystal plane by the surface modifier. At a high reaction temperature, the surface modifiers desorb from the crystal surface, because their kinetic energy exceeds the energy of adsorption. Under such conditions, it becomes advantageous for the inherent structure of the crystal to be thermodynamically stable. Moreover, surface modifiers that are organic molecules decompose at high reaction temperatures.

Although methods for controlling the morphology of fine particles such as metals [1,8,9] and metal-oxide inorganic [2,4,10] compounds have been studied widely, there have been few such studies of metal nitride compounds [11]. This study concerned control of the morphology of metal nitride compounds. Metal nitrides are generally synthesized at temperatures $>350\text{ }^{\circ}\text{C}$ [12,13]. Here my group reported a method that can be used to synthesize metal nitrides, especially copper nitride, at temperatures lower ($<200\text{ }^{\circ}\text{C}$) than those used in conventional methods. My group hypothesized that control of the shape of metal nitride particles can be studied by using this new method. The following is a brief summary of relevant background information.

The focus of this study was the development of a method for preparing copper nitride fine particles and application of that method. Copper nitride has been synthesized using a variety of methods, including solid-phase [14–17] and liquid-phase [18–20] reactions. In the liquid phase, copper nitride fine particles have previously been prepared under harsh conditions: copper chloride and sodium azide in toluene as a solvent were heated in a closed vessel at $185\text{ }^{\circ}\text{C}$ at 4.8 MPa [18], and copper nitrate was heated in 1-octadecylamine at $250\text{ }^{\circ}\text{C}$ [19]. The method described here does not require high temperature and high pressure. For example, copper acetate and ammonia gas were heated in a long-chain alcohol solvent at $190\text{ }^{\circ}\text{C}$ at 1 atm of pressure [21]. Furthermore, my group found that copper nitride fine particles could be prepared using the reaction between copper acetate and urea, without the use of toxic and corrosive gases such as ammonia [22].

The method described here is a facile and safe way to prepare copper nitride fine particles and is characterized by low-temperature ($<200\text{ }^{\circ}\text{C}$) reaction conditions. Thermally mild conditions are advantageous for controlling crystal morphology. On the basis of this consideration, my group synthesized copper nitride fine particles by using different copper sources, such as copper acetate and copper decanoate [23]. The decanoate served as an organic surfactant. The crystallites (primal particles) of copper nitride obtained by preparation with copper acetate and copper decanoate were morphologically cubic and plate-like particles, respectively. The shape of the crystallite of copper nitride was basically anisotropic if a fatty acid copper salt was used as a reagent. In a previous study, my group hypothesized that the alkyl chain length of the fatty acid influences the crystal morphology [23]. However, the extent to which the length of the alkyl moiety influences anisotropy has been unclear. Furthermore, it was unclear why an anisotropic crystal of copper nitride was formed.

In this work, to address these uncertainties, fatty acid copper salts with slightly varying alkyl chain lengths were prepared based on my experience [24], and then the effect of the alkyl chain length on the anisotropy of the nanocrystallite of copper nitride was investigated. In particular, copper nitride was prepared by using fatty acid copper salts with a series of different alkyl chain lengths ranging from $n = 0$ to 12 at n intervals of 1–3 (Figure 1 and Table 1). Direct observations via electron microscopy and characterization by using powder X-ray diffraction with Scherrer analysis were then used to determine how much the length of the alkyl chain influenced the crystal structure of the copper nitride. Finally, the mechanism responsible for the anisotropy of the copper nitride is proposed.

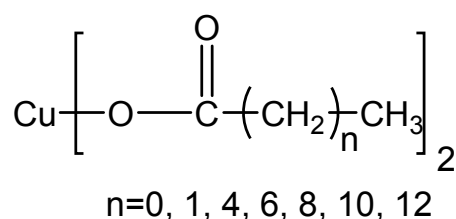


Figure 1. Chemical structure of starting reagents with different alkyl chain lengths.

Table 1. Abbreviations for starting reagents.

IUPAC Name	Common Name	Length of Alkyl Chain	Abbreviation for Reagent
Copper ethanoate	Copper acetate	1	CuC2
Copper propanoate	Copper propionate	2	CuC3
Copper hexanoate	Copper caproate	5	CuC6
Copper octanoate	Copper caprylate	7	CuC8
Copper decanoate	Copper caprinate	9	CuC10
Copper dodecanoate	Copper laurate	11	CuC12
Copper tetradecanoate	Copper myristate	13	CuC14

2. Results

2.1. Observations of Particle and Crystallite Shape

The samples prepared from each fatty acid copper salt reagent were observed by scanning electron microscopy (SEM) and transmission electron microscopy (TEM) to determine the shape of the whole particles as well as the crystallite shape and internal structure of the particles, respectively (Figure 2).

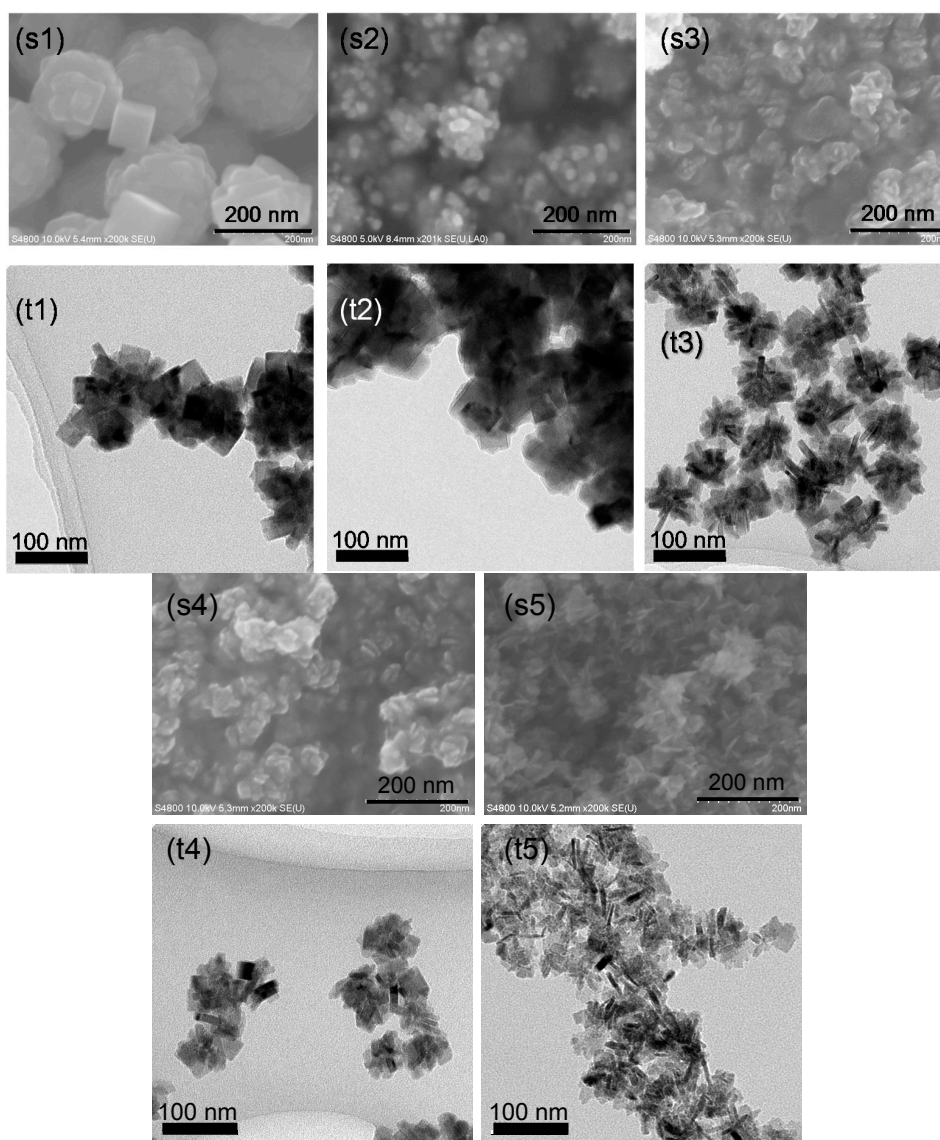


Figure 2. Cont.

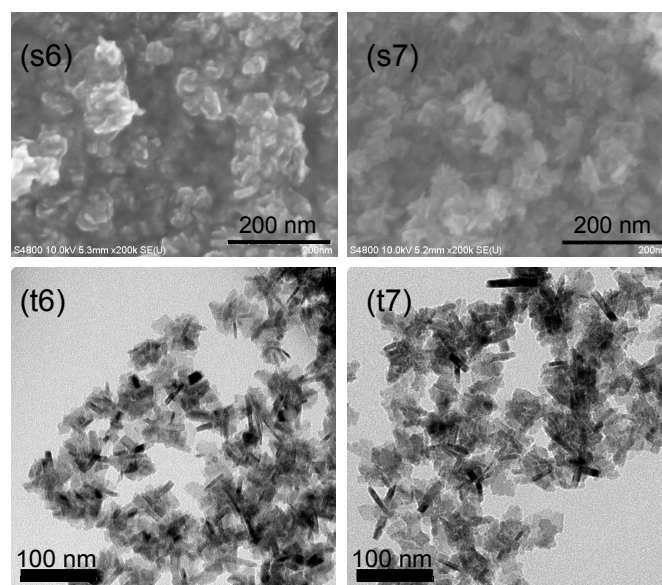


Figure 2. Scanning electron microscopy (SEM) (s) and transmission electron microscopy (TEM) (t) images of the powders prepared from (1) CuC2; (2) CuC3; (3) CuC6; (4) CuC8; (5) CuC10; (6) CuC12; and (7) CuC14 as starting reagents.

For the sample prepared by using CuC2 as a reagent, round particles with diameters of approximately 200 nm were observed by SEM (Figure 2s1). Cubic particles were also observed in some places. The TEM observations (Figure 2t1) revealed round particles that consisted of cubic crystallites. For the sample prepared from CuC3 (Figure 2s2,t2), the particles and crystallites were the same as the particles prepared from CuC2. Namely, use of the CuC3 reagent produced round particles that consisted of cubic crystallites. The SEM image of the particles prepared from CuC3 revealed constituent particles that were clearly distinguishable from the main particle.

For the sample prepared from CuC6, the SEM image revealed constituent particles with plate-like shapes (Figure 2s3). The TEM image (Figure 2t3) revealed aggregate particles that consisted of primary particles with dimensions of approximately 10 and 30 nm in the directions of the short and long axes, respectively. For the sample prepared from CuC8 (Figure 2s4,t4), the morphologies of the secondary and primary particles were similar to those of particles prepared from CuC6.

For the sample prepared from CuC10 (Figure 2s5,t5), the morphology of the primary particles was plate-like but thinner than the particles prepared from CuC6. The dimensions of the primary particles prepared from CuC10 were approximately 5 and 40 nm in the direction of the short and long axes, respectively. Observations of the samples prepared from CuC12 (Figure 2s6,t6) and CuC14 (Figure 2s7,t7) revealed secondary particles that consisted of plate-like particles, similar to the particles prepared from CuC10.

The series of SEM and TEM observations described above revealed that the morphology of the copper nitride fine particles was plate-like when the fatty acid copper salt used to prepare the fine particles had an alkyl-chain length greater than 5. Moreover, the morphology of the plate-like crystallite became thinner when a fatty acid copper salt with an alkyl chain length >9 was used.

2.2. Powder XRD Measurement and Analysis of Crystallite Size

I used a powder x-ray diffractometry (XRD) to characterize the crystal phase of the samples and to analyze crystallite sizes (Figure 3). The XRD patterns were normalized to compare shape of peaks for each obtained pattern. Peaks of all the samples were assigned to copper nitride. The XRD pattern of the sample prepared from CuC2 is described here as a representative example. The XRD pattern showed peaks at 23.466° , 33.367° , 41.180° , 47.895° and 54.070° . These peaks were attributed to

the (100), (110), (111), (200), and (210) planes of copper nitride (PDF2 No. 01-073-6209), respectively. No peaks were attributed to copper, copper oxide(I), or copper oxide(II) in the pattern.

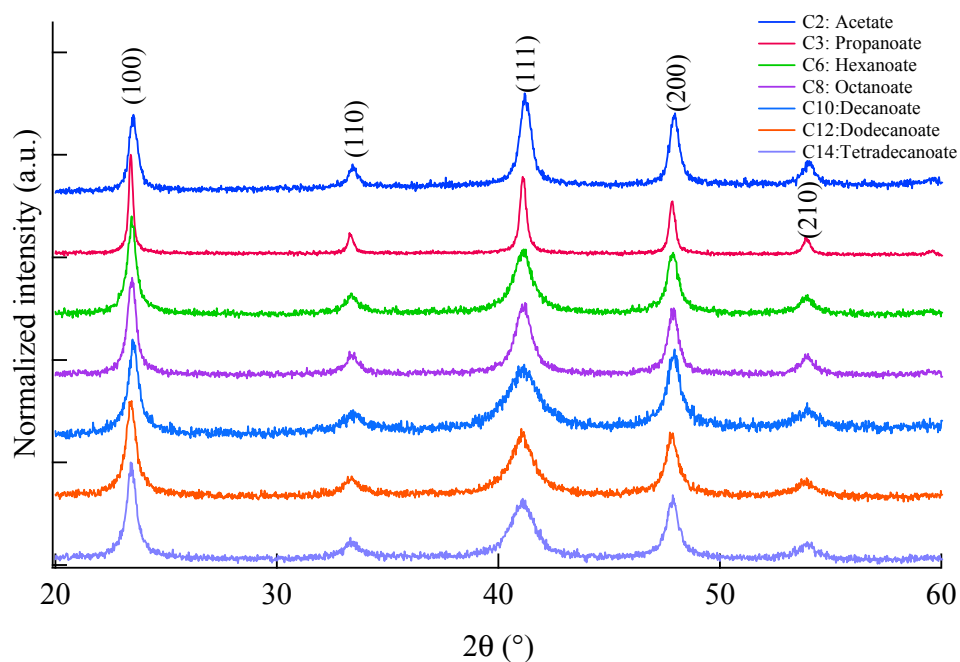


Figure 3. X-ray diffractometry (XRD) patterns of samples prepared from different starting reagents.

Previously crystal structure and planes for (100), (110) and (111) of copper nitride are shown in Figure 4 for ease of imagination.

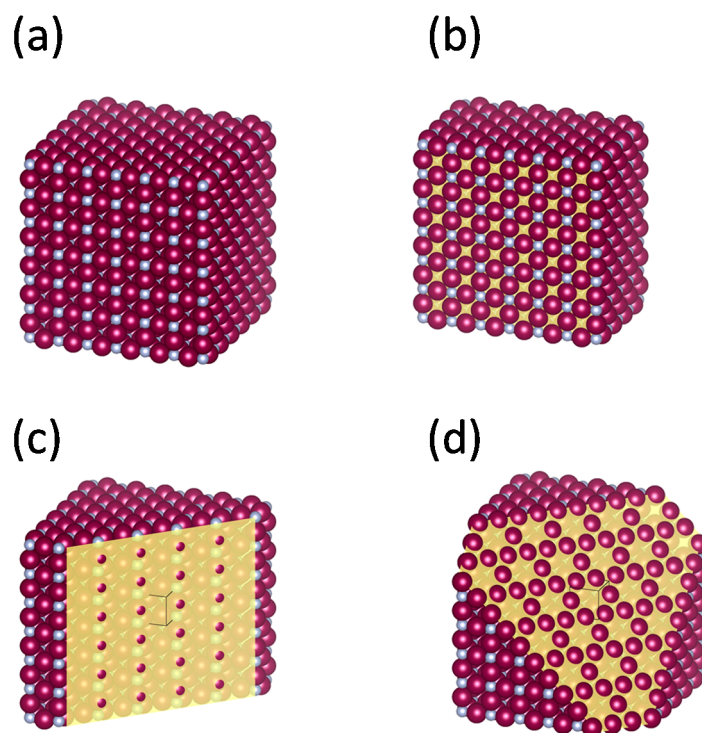


Figure 4. Images of (a) an original crystal structure of copper nitride; (b) a (100) plane; (c) a (110) plane; and (d) a (111) plane.

The peaks in the patterns for the (110), (111) and (210) planes became broader when the alkyl chain length of the fatty acid copper salts was increased. The width of the peak was due to a reduction of crystallite size and increase of the internal strain of the crystallite. My group has previously demonstrated that an increase of the width of the peaks for the nano-crystallite of copper nitride is due to a reduction of the crystallite size [23]. Based on that previous work, crystallite sizes were estimated from full width at half-maximum (FWHM) by using the Scherrer equation after peak fitting with a pseudo-Voigt function.

Table 2 shows estimated peak positions and FWHMs from the peak fitting and calculated lattice spacing and crystallite sizes. The values of the lattice spacing for the (100), (110), (111), (200) and (210) planes differed very little between reagents. The standard errors were less than 0.0002 nm. The crystallite sizes of the copper nitride fine particles prepared by using different reagents decreased when the alkyl chain length of the fatty acid copper salt increased. For each crystal plane, the difference between the largest and smallest crystallite size was less than approximately 18 nm.

Table 2. Estimated values from peak fitting of XRD patterns.

Starting Reagents	2 θ (°)					Lattice Spacing (nm)				
	(100)	(110)	(111)	(200)	(210)	(100)	(110)	(111)	(200)	(210)
CuC2	23.466	33.367	41.180	47.895	54.070	0.3788	0.2683	0.2190	0.1898	0.1695
CuC3	23.384	33.277	41.087	47.810	53.891	0.3801	0.2690	0.2195	0.1901	0.1700
CuC6	23.427	33.335	41.083	47.818	53.930	0.3794	0.2686	0.2195	0.1901	0.1699
CuC8	23.437	33.306	41.088	47.841	53.977	0.3793	0.2688	0.2195	0.1900	0.1697
CuC10	23.500	33.446	41.110	47.885	53.949	0.3783	0.2677	0.2194	0.1898	0.1698
CuC12	23.383	33.288	41.055	47.795	53.752	0.3801	0.2689	0.2197	0.1902	0.1704
CuC14	23.416	33.244	41.065	47.840	53.780	0.3796	0.2693	0.2196	0.1900	0.1703
	FWHM (°)					Crystallite Size (nm)				
	(100)	(110)	(111)	(200)	(210)	(100)	(110)	(111)	(200)	(210)
CuC2	0.4673	0.4909	0.5889	0.4873	0.5771	13.44	11.45	10.67	13.64	11.84
CuC3	0.2050	0.2756	0.2957	0.2523	0.2295	27.08	22.22	19.84	24.09	22.87
CuC6	0.4717	0.6630	1.0092	0.5725	0.6630	11.45	7.87	5.98	10.16	8.11
CuC8	0.4688	0.6607	0.8865	0.5418	0.6299	12.35	8.27	7.07	11.36	10.03
CuC10	0.5617	1.1800	1.7235	0.6904	1.1300	9.25	4.19	3.56	8.25	6.38
CuC12	0.5387	0.8553	1.2636	0.6472	1.0443	9.96	6.17	4.75	8.88	6.16
CuC14	0.5301	0.7867	1.3184	0.6250	0.9190	10.12	6.86	4.79	9.39	7.75
Ratio of the Crystallite Size of Each Crystal Plane to the Crystallite Size of the (100) Plane										
	(100)	(110)	(111)	(200)	(210)					
CuC2	1.00	0.85	0.79	1.01	0.88					
CuC3	1.00	0.82	0.73	0.89	0.84					
CuC6	1.00	0.69	0.52	0.89	0.71					
CuC8	1.00	0.67	0.57	0.92	0.81					
CuC10	1.00	0.45	0.39	0.89	0.69					
CuC12	1.00	0.62	0.48	0.89	0.62					
CuC14	1.00	0.68	0.47	0.93	0.77					

Note: FWHM = full width at half-maximum.

I next compared the ratios of the (100), (110), (111), (200) and (210) crystallite sizes to the crystallite size of the (100) plane (Table 2 and Figure 5). These ratios were significantly less than 1 for the (110), (111) and (210) planes. For the (111) plane, the ratio decreased significantly with increasing alkyl chain length.

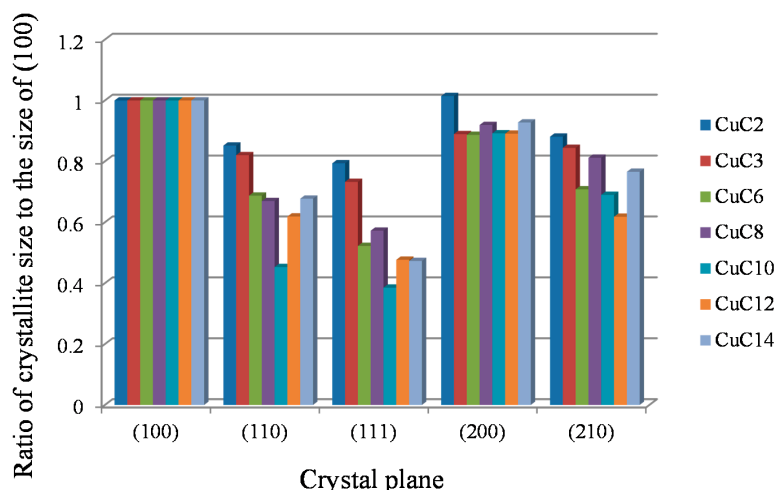


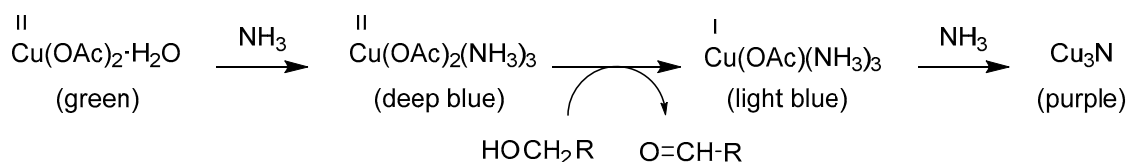
Figure 5. Ratio of size of each crystal plane to the size of the (100) plane.

3. Discussion

Electron microscopic observations of crystallite morphologies and XRD analysis of crystallite sizes and their ratios for each crystal plane showed that the morphology of the copper nitride crystallite was anisotropic when the fine particles were prepared from a fatty acid copper salt with an alkyl chain length exceeding 5 (copper hexanoate). Furthermore, the aspect ratio of the anisotropic shape increased when the fine particles were prepared from a fatty acid copper salt with an alkyl chain length greater than 9 (copper decanoate).

My group hypothesizes that the phenomenon described above can be explained by the fact that crystal growth for a specific plane was inhibited by the surfactant characteristics of the fatty acid. The inhibition of crystal growth and the resultant crystal morphology have been discussed in the context of the copper nitride reaction mechanism previously described in our work [21].

My group has previously proposed the following mechanism (Scheme 1):



Scheme 1. A reaction mechanism to form copper nitride (Ac, acetyl; R, C₈H₁₇). Insert characters indicate solution colors.

The nitridation of copper gave a clear color change as shown in Scheme 1, and the change could be also confirmed in UV-Vis absorption spectrum [21].

Copper acetate monohydrate, which is insoluble in a solvent consisting of a long-chain alcohol, dissolves in the solvent because of formation of an ammine complex due to bubbling of ammonia gas. When the solution is heated to over 120 °C, the copper in the acetate ammine complex is reduced from a bivalent copper ion to a monovalent copper ion by the long-chain alcohol. At the time of the reduction, the ammonia attacks the monovalent copper complex, and, as a result, a bond between the copper atom and nitrogen atom is formed. Copper nitride is formed by sequential progression of the reaction in the solvent.

During this process of nitride formation, the shape of the copper nitride crystal becomes anisotropic due to adsorption of fatty acids on the specific surface of the copper nitride and inhibition of approaching ammonia molecules by the alkyl chain of the fatty acids. Based on this conclusion, I consider that the following phenomena cause the crystallite of copper nitride to be anisotropic:

1. The accession of the ammonia molecule to the crystal surface is inhibited by steric repulsion of the alkyl chain of the fatty acid, which behaves like a surfactant.
2. The fatty acid strongly coordinates on the (110) and the (111) surfaces of copper atoms, for which the atomic length is 0.27 nm.

These two phenomena are discussed in detail below.

The steric barrier increases when the length of the alkyl chain increases. Elaboration of this point is unnecessary because it follows from a basic understanding of chemistry.

Figure 6 indicates the atomic distance between the copper atoms of the copper nitride crystal and the oxygen atoms of the carboxylate. For copper nitride, the atomic distances of 0.38 and 0.27 nm correspond to the lengths of the (100) direction and the (110) direction of the unit cell. For the carboxylate, the distance between the oxygen atoms is 0.226 nm. In comparison to the atomic distances of 0.38 with 0.27 nm for the copper nitride crystal, the carboxylate is strongly coordinated on the surface within a distance of 0.27 nm from the coppers because of the close similarity of the copper–copper and oxygen–oxygen distances.

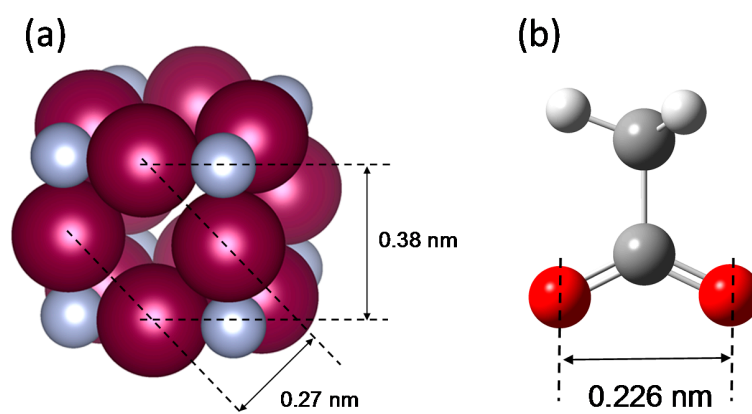


Figure 6. Images of (a) the crystal structure of copper nitride and (b) the molecular structure of the acetate ion.

The coupling between the copper nitride surface and the carboxylate group could be explained by several possible modes, including a unidentate, bidentate, and bridging complex [25]. The coupling form is assigned by using the Δ value of the wavenumber for FT-IR, which was estimated from the difference between the symmetric and asymmetric stretching modes. The Δ values for the unidentate, bidentate, and bridging complex were approximately 200, 50, and 150 cm^{-1} , respectively. For the FT-IR spectrum of copper nitride fine particles in previous work, the wavenumbers attributed to the symmetric and asymmetric stretching modes were 1557 and 1403 cm^{-1} , respectively (in the previous work [21], the wavenumber of 1403 cm^{-1} was misallocated as a deformation vibration of N–H). The Δ value of the carboxylate ion on the copper nitride surface was 154 cm^{-1} . The carboxylate ion coordinates on the surface in the form of a bridge.

Figure 7 shows the relationships between the construction on the crystal surface and the copper and nitrogen atoms that form the next layer for different crystal planes of copper nitride.

For the (100) plane, there are two layers on which the copper atom distances ($L_{\text{Cu-Cu}}$) are 0.38 and 0.27 nm. These layers are designated as the (100)A and (100)B layers, respectively. To grow the next crystal layer, only copper atoms approach the (100)A surface, and the (100)B layer is formed. Copper and nitrogen (derived from ammonia) atoms then approach the (100)B layer, and the (100)A layer is formed.

For the (110) plane, there are two layers designated as (110)A and (110)B. In the case of the (110)A layer, the surface consists of copper atoms separated by a distance of 0.27 nm. The (110)B layer consists of copper atoms separated by two different distances, 0.38 and 0.27 nm. To form the next

crystal layer, copper and nitrogen atoms approach the (110)A layer, and the (110)B layer is formed. Only copper atoms then approach the (110)B layer, and the (110)A layer is formed.

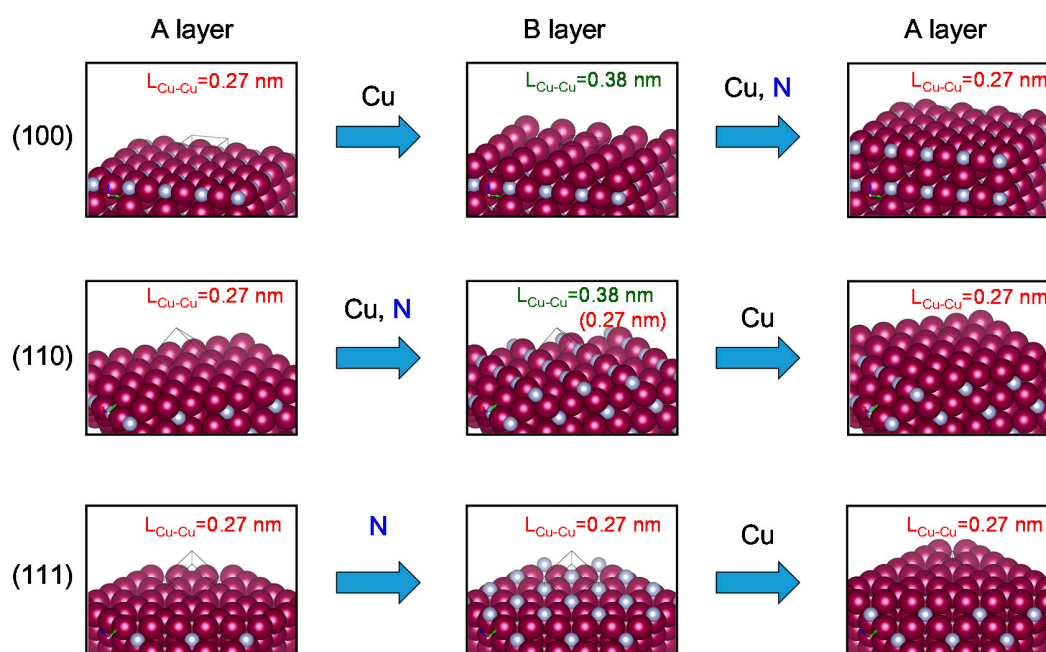


Figure 7. Images of atomic arrays on the (100), (110) and (111) surfaces of copper nitride and elements that form the next crystal layer.

For the (111) plane, there are two layers designated as (111)A and (111)B. The (111)A and (111)B layers consist of only copper and only nitrogen atoms, respectively. For both layers, the copper atoms are 0.27 nm apart. To form the next crystal layer, only nitrogen atoms approach the (111)A layer, and the (111)B layer is formed. To form the next (111)A layer, only copper atoms approach the (111)B layer.

I compared this articulation of the crystal growth of copper nitride with the experimental results. The experimental results revealed that growth of the (110) and (111) planes of the copper nitride crystal were inhibited. For the (110)A and (111)A surfaces, the inhibition was caused by the strong adsorption of fatty acid on the (110) and (111) surfaces, for which the $L_{\text{Cu-Cu}}$ distance was 0.27 nm before the nitride atoms derived from ammonia approached the surfaces.

The anisotropic growth of the copper nitride crystal was thus caused by selective adsorption of the fatty acid and the barrier of the alkyl chain against ammonia.

In future work, I will examine and reveal the adsorption energy between crystal surfaces of copper nitride and surfactants, not only fatty acids but also other surfactants, by means of first-principle calculations and synthetic experiments.

4. Materials and Methods

4.1. Materials

Copper(II) acetate monohydrate (Guaranteed Reagent) and copper(II) propionate monohydrate (>97.5%) were purchased from Kanto Chemical (Tokyo, Japan) and Mitsuwa Chemicals (Osaka, Japan), respectively. Sodium hexanoate (extra pure), sodium octanoate (extra pure), sodium decanoate (extra pure), sodium laurate (extra pure), sodium myristate (extra pure), and 1-nonanol (>97%) were purchased from the Tokyo Chemical Industry (Tokyo, Japan). Copper nitrate trihydrate (>99.5%) was purchased from the Kishida Chemical Company (Osaka, Japan). Ammonia gas (>99.999%)

was purchased from Taiyo Nippon Sanso (Tokyo, Japan). These reagents were used without further purifications.

4.2. Synthesis and Characterization of the Fatty Acid Copper Salt as a Starting Reagent

The fatty acid copper salts used as starting reagents were synthesized in accord with previous works [23,24].

Here I describe the method of preparing copper hexanoate (CuC6). When other starting reagents such as copper octanoate (CuC8), copper decanoate (CuC10), copper dodecanoate (CuC12), and copper tetradecanoate (CuC14) were synthesized, the fatty acid sodium salts were changed to the fatty acid sodium salts with the appropriate alkyl chain length.

Sodium hexanoate (51 mmol) was completely dissolved in deionized water (400 mL) at 80 °C. Copper(II) nitrate trihydrate (25 mmol) in deionized water (100 mL) was added to the solution. Green precipitates were immediately formed. The precipitates were collected by filtration, washed with deionized water, and then washed with methanol. A green powder was obtained after drying the precipitates by heating at 60 °C for 12 h under a vacuum.

The molecular weight of the product was measured by using matrix-assisted laser desorption/ionization time-of-flight mass spectroscopy (MALDI-TOF MS) with an autoflex speed MALDI-TOF/TOF mass spectrometer (Bruker Daltonics, Billerica, MA, USA) operated in a reflector mode. The matrix was 9-Nitroanthracene. The spectrum was recorded in a negative ion mode.

The Fourier transform infrared spectrum was measured with a Spectrum 1000 instrument (PerkinElmer Inc., Waltham, MA, USA) equipped with a Universal attenuated total reflection (ATR) sampling instrument (PerkinElmer). The spectrum was recorded at room temperature from 650 to 4000 cm^{-1} with a spectral resolution of 2 cm^{-1} .

Elemental analysis was carried out with an EA 1110 instrument (CE Instruments, Wigan, UK) for carbon and hydrogen. Oxygen was measured using a Flash EA 1112 instrument (CE Instruments).

Copper hexanoate (CuC6). Analytical data. 50% yield; MALDI-TOF (m/z): $[\text{M}]^-$ calculated for $\text{C}_{12}\text{H}_{22}\text{CuO}_4$, 293.09; found, 293.10 FT-IR (ATR method): 2929 (CH_3), 2859 (CH_2), 1565 (COO), 1532, 1464, 1414, 1344, 1303, 1070, and 1035 cm^{-1} . Theoretical composition of $\text{C}_{12}\text{H}_{22}\text{CuO}_4$: C, 49.05; H, 7.55; O, 21.78%. Found: C, 46.37; H, 7.20; O, 22.47%.

Copper octanoate (CuC8). Analytical data. 56% yield; MALDI-TOF (m/z): $[\text{M}]^-$ calculated for $\text{C}_{16}\text{H}_{30}\text{CuO}_4$, 349.15; found, 349.25. FT-IR (ATR method): 2924 (CH_3), 2854 (CH_2), 1569 (COO), 1413, 1378, 1343, 1302, 1069, and 1033 cm^{-1} . Theoretical composition of $\text{C}_{16}\text{H}_{30}\text{CuO}_4$: C, 54.91; H, 8.64; O, 18.29%. Found: C, 45.70; H, 7.48; O, 20.54%.

Copper decanoate (CuC10). Analytical data. 92% yield; MALDI-TOF (m/z): $[\text{M}]^-$ calculated for $\text{C}_{20}\text{H}_{38}\text{CuO}_4$, 405.22; found, 405.29. FT-IR (ATR method): 2915 (CH_3), 2849 (CH_2), 1580 (COO), 1488–1384 (CH_3 , CH_2), 1340, 1316, 1301, 1276, 1070, 1035, 1014, 888, and 877 cm^{-1} . Theoretical composition of $\text{C}_{20}\text{H}_{38}\text{CuO}_4$: C, 59.16; H, 9.43; O, 15.76%. Found: C, 58.64; H, 9.30; O, 15.81%.

Copper dodecanoate (CuC12). Analytical data. 95% yield; MALDI-TOF (m/z): $[\text{M}]^-$ calculated for $\text{C}_{24}\text{H}_{46}\text{CuO}_4$, 461.28; found, 461.33. FT-IR (ATR method): 2915 (CH_3), 2849 (CH_2), 1581 (COO), 1467, 1422, 1317, 1116, and 1069 cm^{-1} . Theoretical composition of $\text{C}_{24}\text{H}_{46}\text{CuO}_4$: C, 62.37; H, 10.03; O, 13.85%. Found: C, 61.86; H, 9.90; O, 13.88%.

Copper tetradecanoate (CuC14). Analytical data. 95% yield; MALDI-TOF (m/z): $[\text{M}]^-$ calculated for $\text{C}_{28}\text{H}_{54}\text{CuO}_4$, 517.34; found, 517.35. FT-IR (ATR method): 2913 (CH_3), 2849 (CH_2), 1582 (COO), 1513, 1467, 1436, 1422, 1317, and 1118 cm^{-1} . Theoretical composition of $\text{C}_{28}\text{H}_{54}\text{CuO}_4$: C, 64.89; H, 10.50; O, 12.35%. Found: C, 64.91; H, 10.43; O, 12.24%.

4.3. Preparation and Characterization of Copper Nitride Fine Particles

Copper nitride fine particles were prepared in accord with a previous report [21] with modifications. Specifically, the copper acetate starting reagent was changed to synthesized fatty acid copper salts.

A dispersion of copper acetate monohydrate (2 mmol) in 1-nonanol (400 mL) was bubbled with ammonia (100 mL/min) and heated at 190 °C for 40 min (ramp time, 10 min; hold time, 30 min) in a μ Reactor Ex microwave heater (2.45 GHz, Shikoku Instrumentation, Kagawa, Japan) equipped with a fiber-optic thermometer (AMOTH FL-2000, Anritsu Meter, Tokyo, Japan). The temperature of the solution was controlled by automatically changing the microwave power. The opaque brown liquid that was obtained from the reaction was super-centrifuged (30,000 g for 60 min) to yield a brown powder, which was washed three times with *n*-hexane.

The powders that were obtained were characterized by using XRD, SEM and TEM. The crystal structures were determined by using a SmartLab (Rigaku, Tokyo, Japan) with Cu K α radiation at 40 kV and 30 mA at $2\theta = 20^\circ$ – 90° . The morphology of the powder was observed by using an S-4800 microscope (Hitachi High-Technologies, Tokyo, Japan) with an acceleration voltage of 2 kV, an emission current of 10 μ A, and a working distance of 3 mm. The morphology of the powder was also observed by using a TECNAI G20 microscope (FEI, Hillsboro, OR, USA) with an acceleration voltage of 200 kV.

5. Conclusions

A crystallite of copper nitride with an anisotropic shape was prepared by using a method to synthesize copper nitride fine particles under mild conditions. Changing the alkyl chain length of the fatty acid allowed me to examine the effect of the chain length on the anisotropy. The results showed that the anisotropic nature of the crystallite was expressed when the length of the fatty acid chain exceeded 5. Based on the experimental results, I considered when anisotropy occurred and concluded that formation of the anisotropic crystallite of copper nitride was caused by the following phenomena:

1. The accession of ammonia molecules to the crystal surface was inhibited by steric repulsion of the alkyl chain of the fatty acid, which functioned as a surfactant.
2. The fatty acid strongly coordinated on the (110) and the (111) surfaces of the copper atoms, the atomic length of which was 0.27 nm.

Acknowledgments: This work was financially supported by a grant from the A-STEP (Adaptable and Seamless Technology Transfer Program through Target-Driven R&D) program of the Japan Science and Technology Agency (feasibility study stage, No. AS232Z00276C).

Conflicts of Interest: The authors declare no conflict of interest.

Abbreviations

The following abbreviations are used in this manuscript:

ATR	attenuated total reflection
FWHM	full width at half-maximum
MALDI-TOF MS	matrix-assisted laser desorption/ionization time-of-flight mass spectroscopy
SEM	scanning electron microscopy
TEM	transmission electron microscopy
XRD	x-ray diffractometry

References

1. Zhang, H.; Jin, M.S.; Xiong, Y.J.; Lim, B.; Xia, Y.N. Shape-controlled synthesis of Pd nanocrystals and their catalytic applications. *Acc. Chem. Res.* **2013**, *46*, 1783–1794. [[CrossRef](#)] [[PubMed](#)]
2. Huang, W.X. Crystal plane-dependent surface reactivity and catalytic property of oxide catalysts studied with oxide nanocrystal model catalysts. *Top. Catal.* **2013**, *56*, 1363–1376. [[CrossRef](#)]

3. Bensebaa, F. Clean energy. In *Interface Science and Technology*; Farid, B., Ed.; Elsevier: Amsterdam, The Netherlands, 2013; Volume 19, pp. 279–383.
4. Feng, W.L.; Huang, P.; Wang, B.C.; Wang, C.W.; Wang, W.G.; Wang, T.L.; Chen, S.F.; Lv, R.L.; Qin, Y.H.; Ma, J.Y. Solvothermal synthesis of ZnO with different morphologies in dimethylacetamide media. *Ceram. Int.* **2016**, *42*, 2250–2256. [[CrossRef](#)]
5. Chen, R.R.; Han, B.N.; Yang, L.; Yang, Y.M.; Xu, Y.; Mai, Y.H. Controllable synthesis and characterization of CdS quantum dots by a microemulsion-mediated hydrothermal method. *J. Lumin.* **2016**, *172*, 197–200. [[CrossRef](#)]
6. Bensebaa, F. Optoelectronics. In *Interface Science and Technology*; Farid, B., Ed.; Elsevier: Amsterdam, The Netherlands, 2013; Volume 19, pp. 429–479.
7. Turco Liveri, V. *Controlled Synthesis of Nanoparticles in Microheterogeneous Systems*; Springer: Berlin, Germany, 2006.
8. Grzelczak, M.; Pérez-Juste, J.; Mulvaney, P.; Liz-Marzán, L.M. Shape control in gold nanoparticle synthesis. *Chem. Soc. Rev.* **2008**, *37*, 1783–1791. [[CrossRef](#)]
9. Yarulin, A.; Yuranov, I.; Cárdenas-Lizana, F.; Abdulkin, P.; Kiwi-Minsker, L. Size-effect of Pd-(poly(*N*-vinyl-2-pyrrolidone)) nanocatalysts on selective hydrogenation of alkynols with different alkyl chains. *J. Phys. Chem. C* **2013**, *117*, 13424–13434. [[CrossRef](#)]
10. Liu, J.; Jin, J.; Deng, Z.; Huang, S.Z.; Hu, Z.Y.; Wang, L.; Wang, C.; Chen, L.H.; Li, Y.; Van Tendeloo, G.; et al. Tailoring CuO nanostructures for enhanced photocatalytic property. *J. Colloid Interface Sci.* **2012**, *384*, 1–9. [[CrossRef](#)] [[PubMed](#)]
11. Yin, J.; Yu, J.; Li, X.M.; Li, J.D.; Zhou, J.X.; Zhang, Z.H.; Guo, W.L. Large single-crystal hexagonal boron nitride monolayer domains with controlled morphology and straight merging boundaries. *Small* **2015**, *11*, 4497–4502. [[CrossRef](#)] [[PubMed](#)]
12. Chirico, P.; Hector, A.L.; Mazumder, B. Solvothermal synthesis of group 5 and 6 nitrides via reactions using LiNH₂ and ammonia nitrogen sources. *Dalton Trans.* **2010**, *39*, 6092–6097. [[CrossRef](#)] [[PubMed](#)]
13. Choi, D.; Kumta, P.N. Synthesis, structure, and electrochemical characterization of nanocrystalline tantalum and tungsten nitrides. *J. Am. Ceram. Soc.* **2007**, *90*, 3113–3120. [[CrossRef](#)]
14. Juza, R.; Hahn, H. Crystal structures of Cu₃N, GaN and InN—Metallic amides and metallic nitrides. *Z. Anorg. Allg. Chem.* **1938**, *239*, 282–287. [[CrossRef](#)]
15. Juza, R. Remarks on the crystal structure of Cu₃N. *Z. Anorg. Allg. Chem.* **1941**, *248*, 118–120. [[CrossRef](#)]
16. Li, X.J.; Hector, A.L.; Owen, J.R. Evaluation of Cu₃N and CuO as negative electrode materials for sodium batteries. *J. Phys. Chem. C* **2014**, *118*, 29568–29573. [[CrossRef](#)]
17. Szczyński, R.; Szyk, E.; Wiśniewski, M.A.; Hoang, T.K.A.; Gregory, D.H. Facile preparation of copper nitride powders and nanostructured films. *J. Mater. Chem. C* **2016**, *4*, 5031–5037. [[CrossRef](#)]
18. Choi, J.L.; Gillan, E.G. Solvothermal synthesis of nanocrystalline copper nitride from an energetically unstable copper azide precursor. *Inorg. Chem.* **2005**, *44*, 7385–7393. [[CrossRef](#)] [[PubMed](#)]
19. Wu, H.; Chen, W. Copper nitride nanocubes: Size-controlled synthesis and application as cathode catalyst in alkaline fuel cells. *J. Am. Chem. Soc.* **2011**, *133*, 15236–15239. [[CrossRef](#)] [[PubMed](#)]
20. Wang, D.; Li, Y. Controllable synthesis of Cu-based nanocrystals in ODA solvent. *Chem. Commun.* **2011**, *47*, 3604–3606. [[CrossRef](#)] [[PubMed](#)]
21. Nakamura, T.; Hayashi, H.; Hanaoka, T.; Ebina, T. Preparation of copper nitride (Cu₃N) nanoparticles in long-chain alcohols at 130–200 °C and nitridation mechanism. *Inorg. Chem.* **2014**, *53*, 710–715. [[CrossRef](#)] [[PubMed](#)]
22. Nakamura, T.; Hayashi, H.; Ebina, T. Preparation of copper nitride nanoparticles using urea as a nitrogen source in a long-chain alcohol. *J. Nanopart. Res.* **2014**, *16*, 2699. [[CrossRef](#)]
23. Nakamura, T.; Hiyoshi, N.; Hayashi, H.; Ebina, T. Preparation of plate-like copper nitride nanoparticles from a fatty acid copper(II) salt and detailed observations by high resolution transmission electron microscopy and high-angle annular dark-field scanning transmission electron microscopy. *Mater. Lett.* **2015**, *139*, 271–274. [[CrossRef](#)]
24. Nakamura, T.; Tsukahara, Y.; Sakata, T.; Mori, H.; Kanbe, Y.; Bessho, H.; Wada, Y. Preparation of monodispersed Cu nanoparticles by microwave-assisted alcohol reduction. *Bull. Chem. Soc. Jpn.* **2007**, *80*, 224–232. [[CrossRef](#)]

25. Nakamoto, K. *Infrared and Raman Spectra of Inorganic and Coordination Compounds*, 5th ed.; Wiley: New York, NY, USA, 1997.



© 2017 by the author; licensee MDPI, Basel, Switzerland. This article is an open access article distributed under the terms and conditions of the Creative Commons Attribution (CC-BY) license (<http://creativecommons.org/licenses/by/4.0/>).